AIAA JOURNAL
Vol. 31, No. 4, April 1993

Outflow Boundary Conditions for Spatial Navier-Stokes Simulations of Transition Boundary Layers

M. Kloker* and U. Konzelmann*
Universität Stuttgart, 7000 Stuttgart 80, Germany
and
H. Fasel†
University of Arizona, Tucson, Arizona 85721

For numerical simulations of the spatially evolving laminar-turbulent transition process in boundary layers using the complete Navier-Stokes equations, the treatment of the outflow boundary requires special attention. The disturbances must pass through this boundary without causing reflections that would significantly alter the flow upstream. In this paper, we present various methods to influence the disturbed flow downstream of the region of interest, such that the disturbance level at the outflow boundary is significantly reduced, and hence the possibility of reflections is minimized. To demonstrate the effectiveness of the various techniques to alter the disturbance flow near the outflow boundary, the fundamental breakdown of a strongly decelerated boundary layer is simulated. Our results show that the most effective method is to spatially suppress the disturbance vorticity within a so-called "relaminarization zone." The suppression of the disturbance vorticity is gradually imposed within this zone by means of a weighting function. The enforced decay of the disturbance vorticity leads to a practically complete dissipation of any fluctuating component. Most importantly, this technique causes only a negligible upstream effect. The "relaminarized" boundary-layer flow then passes through the outflow boundary without significant reflections.

I. Introduction

IN the literature, most numerical simulations of laminar-turbulent transition phenomena are based on the so-called temporal model. In this model, the flow is assumed to be spatially periodic in the downstream direction so that periodic boundary conditions can be employed at the inflow and outflow boundaries, i.e., inflow quantities for both the base flow and the disturbance flow are identical at the inflow and outflow boundaries. The spatial periodicity allows efficient use of (pseudo) spectral approximations in the downstream direction. In addition to allowing a small spatial integration domain containing only one wavelength, this enables simulations that are relatively inexpensive with respect to both required computer memory and time. Because of the forced spatial periodicity, the disturbances evolve in time, and a characteristic velocity, usually the phase velocity, has to be used to compare the numerical results with those observed in the spatial disturbance development of experiments. Applied to simulations of transition phenomena in plane Poiseuille flow and zero pressure gradient boundary layers, this model yields good qualitative agreement with experiments (see Kleiser and Zang[1]).

For boundary-layer flows with a more pronounced downstream variation, e.g., boundary layers with pressure gradients and/or local suction at the wall, the assumptions in the temporal model are no longer justifiable. For such flows, the so-called spatial model should be used for realistic transition simulation. However, compared with the temporal approach, use of the spatial model introduces two major difficulties.

1) Since the transition process extends over a large downstream region, a large downstream integration domain is required, in contrast to the one-wavelength domain for the temporal model. Consequently, the computational cost is significantly higher with respect to both computation time and storage requirements.

2) Boundary conditions for the outflow boundary have to be specified and implemented into the numerical model, such that even the nonperiodic, large-amplitude fluctuations resulting from the breakdown process can pass through this boundary without causing unphysical upstream effects.

Physical and unphysical upstream effects are central to the problem. For incompresible flows, *physical* directional influence, even against the mean flow, is understandable[2] when the divergence of the vector momentum equation is taken, yielding

$$\nabla^2 p = \rho \frac{\partial^2 (u_i u_j)}{\partial x_i \partial x_j} = \text{local source at point } x_i \qquad (1)$$

Clearly, superposable pressure fields are generated in the field when the derivative products are nonzero, as will be the case in

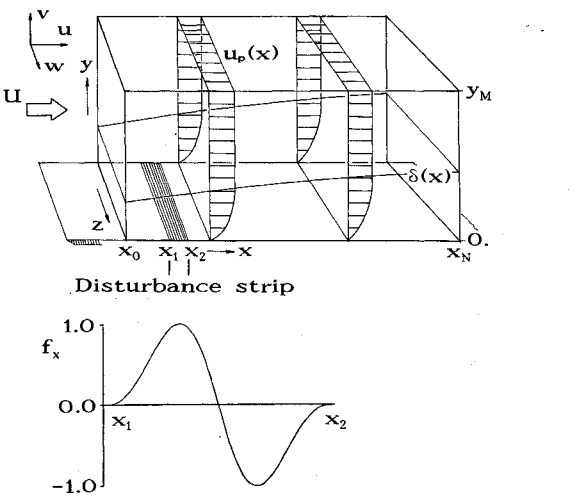

Fig. 1 Integration domain and function f_x for the disturbance generation by blowing and suction.

Received April 23, 1991; revision received July 2, 1992; accepted for publication July 6, 1992.

*Research Assistant, Institut für Aerodynamik und Gasdynamik, Ppaffenwaldring 21.

†Professor, Department of Aerospace and Mechanical Engineering. Member AIAA.

the nonlinear stages of primary and higher instabilities. For nearly parallel flows, the dominant physical source in the early stages is linearizable around the base flow u_B, yielding $-2\rho(\partial u_B/\partial y)(\partial v'/\partial x)$ for the local p' source. Here, the primes indicate perturbations around the base flow. Buell and Huerre[2] express p in the form of an integral equation in terms of the Green's function of the elliptic Poisson equation and show how terms in the surface integral over the finite integration domain cause *unphysical* reflections of the *physical* sources within the domain.

As an example, let us consider the conditions at the inflow boundary at x_0 of Fig. 1, which is usually far from the amplified sources near the breakdown. If we would, for example, prescribe the velocity fluctuations at x_0, we would force the gradient of the pressure field due to the sources in Eq. (1) to be zero at that plane, which is seldom true. However, the sources in Eq. (1) are of the quadrupole type (except at solid walls where they are of the dipole type). As such, their fields decay rapidly with distance from the source. Thus the motion induced by grad p, which is suppressed (and thereby reflected) by the prescribed boundary condition at x_0, is likely to be so small as to be below the resolution of numerical and/or physical "measuring instruments" near x_0.

The situation is vastly different at the outflow boundary x_N of Fig. 1, which may cut right through the largest convected vortical disturbances. This situation is reminiscent of the "edge-tone" phenomenon in a jet flow, where a solid streamwise boundary interferes with convected large eddies and thereby generates strong dipole sources. These in turn radiate to the "inflow boundary" at the "jet lips" and establish a self-excited (globally unstable) system. The prescribed outflow conditions over the plane x_N interfere similarly with the otherwise unhindered vorticity field, thus generating dipole-like sources that radiate unphysically into the domain.[3] In fact, coupling of these disturbances with inflow boundary conditions may lead to unphysical self-excited, regular or chaotic flowfields, e.g., Buell and Huerre[2] and Grinstein et al.,[4] in the case of free mixing layers. In our problem, the pressure of the (damping) wall at $y = 0$ makes the situation less extreme but important nevertheless.

Based on our extensive experience in spatial simulations for various flow geometries, we feel that conditions that are completely satisfactory and fairly general to work for different situations are very difficult to find. One way to bypass the need for proper outflow boundary conditions is to use an integration domain such that the outflow boundary is always ahead of the vorticity disturbance front (see Fasel et al.[5] and Konzelmann et al.[6]), which varies with the initial disturbance startup. Thus, the convected vortical disturbances do not reach the outflow boundary. The wave front breaks down in a high-frequency random motion not unlike the experimental situation. This random region is growing rapidly as time goes on, and therefore the outflow boundary has to be moved farther and farther downstream. In a realistic breakdown simulation, the random region finally extends to about two-thirds of the integration domain. Therefore, the computational time and memory requirements grow nonlinearly when the domain of interest is increased. This approach may be criticized on two counts: 1) the largest sources in Eq. (1) occur near the transient vorticity disturbance front, which is dependent on the initial conditions, and therefore the unphysical reflections of these large near-outflow sources could be significant; and 2) no rigorous operational criteria have yet been proposed to test how much of the computed field is independent of the initial conditions and the dipole outflow reflections.

The propagation and spreading of the random domain suggest a different strategy to deal with the outflow region. In this strategy, the physical location of the outflow boundary is moved far downstream by employing a rapidly expanding computational grid. In addition to being able to move the outflow boundary far downstream with a few grid points, the idea is that the small-scale random motion would be grossly under-resolved in this coarse grid and would therefore not develop downstream as before but, rather, would be damped out. First attempts to implement this idea, however, did not yield satisfactory results. Therefore this approach requires further detailed investigations and is currently the subject of ongoing research. In any case, use of a nonuniform grid would increase computation time and/or memory requirements.

A different approach to deal with the outflow boundary conditions is based on using physical mechanisms to stabilize the boundary-layer flow in a region near the outflow boundary, i.e., to introduce a so-called relaminarization zone. The goal of this strategy is to drastically reduce the disturbance amplitudes in this region so that undue reflections would be reduced accordingly. For small disturbance amplitudes, boundary conditions can be specified and implemented into a Navier-Stokes code, causing only negligible upstream influence, as shown by Fasel et al.[5] Favorable pressure gradients or local suction at the wall can be employed as physical means to stabilize the flow. These measures are known to highly stabilize the boundary layer, at least with respect to small amplitude disturbances. Another viable tool would be to increase the viscosity locally (far beyond levels where viscosity is known to be destabilizing) to make the conditions near the outflow subcritical.

In this paper, attempts to incorporate this strategy of using a stabilization zone near the outflow boundary for transition simulations based on the complete Navier-Stokes equations are discussed. To demonstrate the efficiency of the various methods of stabilization, the simulation of a fundamental breakdown in a strongly decelerated flat plate-boundary layer was chosen as a test case. Using this test case was advantageous for two reasons. First, the amplitude levels before breakdown are larger than, for example, for zero and negative pressure gradients. In addition, the pressure feedback is stronger than for the zero and negative pressure gradient cases. This case therefore represents a much more stringent test with regard to the effectiveness of the various stabilization techniques. Second, the large amplitudes are attained within a relatively short distance downstream of the disturbance generation. Thus these calculations can be carried out with a much smaller domain than for a case with zero pressure gradient, thereby minimizing the computational cost.

As will be seen, we found that increasing the viscosity locally was most effective but still not satisfactory. However, based on the experience from these investigations, we were led to a rather effective method to drastically reduce the disturbance level within a relatively small "relaminarization zone." Within this outflow region, the vorticity components of the fluctuations are gradually suppressed in the downstream direction. This leads to a practically complete dissipation of any fluctuation component at the end of the relaminarization zone. This approach results in minimal upstream effects and can be numerically implemented at no additional cost.

A different but somewhat related method was suggested by Spalart[7] for a spatial transition simulation using the streamwise periodic model. By applying a forcing function on the longitudinal velocity component of a steady stagnation point flow, he was able to use periodic boundary conditions for the two outflow boundaries in the simulation of the unsteady disturbed flow. However, a part of the base flow was also suppressed and not only the disturbance flow as in our relaminarization technique. Later, Spalart[8] extended his method to realistic inflow-outflow problems by superimposing (in the "fringes" of the computational domain) a disturbance decay on the base flow. Source terms are added on the right-hand sides of the momentum equations to avoid the re-entering of disturbances into the streamwise quasiperiodic domain.

The techniques to reduce the disturbance level through relaminarization zones invariably introduce nonhomogeneous changes in the basic differential equation system either gradually or at discrete surfaces, or both. In other words, they are

equivalent to effective spatial (or time) dependence of the coefficients of the differential operators. Such effective variation of properties of the medium generates partial internal reflections and upstream influences, which are very difficult to estimate analytically. When the variation is gradual, the reflections are expected to be very weak, no worse than quadrupole like. We are, in fact, testing if they are minor, not by analysis, but through comparing numerical results obtained from our numerical difference scheme. The unphysical influence field from these artificial sources also decays with distance, so it should not contaminate the basic physical mechanisms in the regions of interest.

II. Numerical Method

The numerical method is based on the work of Fasel et al.[5] This method has been successfully applied to various transition studies, albeit with a more or less extended streamwise integration domain as discussed previously. The Navier-Stokes equations are solved in a rectangular integration domain, shown schematically in Fig. 1. The downstream direction is x, the direction normal to the plate is y, and the spanwise direction is z. The velocity components are u, v, and w. All variables are nondimensionalized with a reference length L and the freestream velocity U_∞. The nondimensional variables relate to the corresponding dimensional ones (denoted by bars) as

$$x = \frac{\bar{x}}{L}, \quad y = \frac{\bar{y}}{L}\sqrt{Re}, \quad z = \frac{\bar{z}}{L}, \quad t = \bar{t}\frac{U_\infty}{L}$$
$$u = \frac{\bar{u}}{U_\infty}, \quad v = \frac{\bar{v}}{U_\infty}\sqrt{Re}, \quad w = \frac{\bar{w}}{U_\infty} \tag{2}$$

The Reynolds number is $Re = U_\infty(L/\nu)$, where ν is the kinematic viscosity. The three vorticity components are defined as

$$\omega_x = \frac{1}{Re}\frac{\partial v}{\partial x} - \frac{\partial w}{\partial y}$$
$$\omega_y = \frac{\partial w}{\partial z} - \frac{\partial u}{\partial z} \tag{3}$$
$$\omega_z = \frac{\partial u}{\partial y} - \frac{1}{Re}\frac{\partial v}{\partial x}$$

The flow variables are decomposed into those of the two-dimensional base flow (index B) and of the disturbance flow (denoted by a prime):

$$u = u_B + u'$$
$$v = v_b + v' \tag{4}$$
$$w = w'$$

To calculate the base flow, the Navier-Stokes equations are used in a vorticity-velocity formulation[9] with a vorticity transport equation for ω_{zB},

$$\frac{\partial}{\partial x}(u_B\omega_{zB}) + \frac{\partial}{\partial y}(v_B\omega_{zB}) = \frac{1}{Re}\frac{\partial^2\omega_{zB}}{\partial x^2} + \frac{\partial^2\omega_{zB}}{\partial y^2} \tag{5a}$$

a Poisson-type equation for v_B,

$$\frac{1}{Re}\frac{\partial^2 v_B}{\partial x^2} + \frac{\partial^2 v_B}{\partial y^2} = -\frac{\partial\omega_{zB}}{\partial x} \tag{5b}$$

and for u_B,

$$\frac{\partial^2 u_B}{\partial x^2} = -\frac{\partial^2 v_B}{\partial x\,\partial y} \tag{5c}$$

The base flow is calculated in the rectangular integration domain using the following boundary conditions. At the inflow boundary ($x = x_0$), Falkner-Skan boundary-layer profiles (index FS) are specified as

$$u_B(x_0, y) = u_{FS}(y)$$
$$v_B(x_0, y) = v_{FS}(y) \tag{6}$$
$$\omega_{zB}(x_0, y) = \omega_{zFS}(y)$$

At the wall, the conditions

$$u_B(x, 0) = 0 \tag{7a}$$
$$v_B(x, 0) = f_B(x) \tag{7b}$$
$$\left.\frac{\partial v_B}{\partial y}\right|_{x,0} = 0 \tag{7c}$$

are used. Thus, timewise constant suction can be applied to stabilize the base flow. The wall vorticity is calculated from

$$\left.\frac{\partial\omega_{zB}}{\partial x}\right|_{x,0} = -\left.\frac{\partial^2 v_B}{\partial y^2}\right|_{x,0} - \frac{1}{Re}\left.\frac{\partial^2 v_B}{\partial x^2}\right|_{x,0} \tag{7d}$$

At the outflow boundary ($x = x_N$), Eqs. (5a) and (5b) are solved using

$$\frac{1}{Re}\left.\frac{\partial^2\omega_{zB}}{\partial x^2}\right|_{x_N,y} = 0 \tag{8a}$$

and

$$\frac{1}{Re}\left.\frac{\partial^2 v_B}{\partial x^2}\right|_{x_N,y} = 0 \tag{8b}$$

whereas u_B is calculated from the Poisson-type equation

$$\frac{1}{Re}\frac{\partial^2 u_B}{\partial x^2} + \frac{\partial^2 u_B}{\partial y^2} = \frac{\partial\omega_{zB}}{\partial y} \tag{8c}$$

with

$$\frac{1}{Re}\left.\frac{\partial^2 u_B}{\partial x^2}\right|_{x_N,y} = 0 \tag{8d}$$

The freestream boundary ($y = y_M$) is far enough from the wall so that potential flow can be assumed with

$$\omega_{zB}(x, y_M) = 0 \tag{9a}$$

u_B is prescribed according to a given streamwise pressure gradient,

$$u_B(x, y_M) = u_P(x) \tag{9b}$$

and v_B is calculated from the continuity equation,

$$\left.\frac{\partial v_B}{\partial y}\right|_{x,y_M} = -\frac{du_P}{dx} \tag{9c}$$

The equations are discretized with finite differences of fourth-order accuracy in the x and y directions. The vorticity transport equation is solved with a pseudo-unsteady time-marching technique: the derivatives with respect to y are treated explicitly (Euler forward), and the x direction is treated implicitly (Euler backward). The v_B-Poisson equation is solved with a vectorizable, stripe pattern Gauss-Seidel-like line iteration, and the u_B equation is directly solved.

The calculation of the disturbance flow is based on three vorticity transport equations for the vorticity components

$$\frac{\partial \omega_x'}{\partial t} + \frac{\partial}{\partial y}(v'\omega_x' - u'\omega_y' + v_B\omega_x' - u_B\omega_y') - \frac{\partial}{\partial z}(u'\omega_z' - w'\omega_x' + u_B\omega_z' + u'\omega_{zB}) = \tilde{\Delta}\omega_x' \tag{10a}$$

$$\frac{\partial \omega_y'}{\partial t} - \frac{\partial}{\partial x}(v'\omega_x' - u'\omega_y' + v_B\omega_x' - u_B\omega_y') + \frac{\partial}{\partial z}(w'\omega_y' - v'\omega_z' - v_B\omega_z' - v'\omega_{zB}) = \tilde{\Delta}\omega_y' \tag{10b}$$

$$\frac{\partial \omega_z'}{\partial t} + \frac{\partial}{\partial x}(u'\omega_z' - w'\omega_x' + u_B\omega_z' + u'\omega_{zB}) - \frac{\partial}{\partial y}(w'\omega_y' - v'\omega_z' - v_B\omega_z' - v'\omega_{zB}) = \tilde{\Delta}\omega_z' \tag{10c}$$

and three Poisson-type equations

$$\frac{\partial^2 u'}{\partial x^2} + \frac{\partial^2 u'}{\partial z^2} = -\frac{\partial \omega_y'}{\partial z} - \frac{\partial^2 v'}{\partial x \partial y} \tag{10d}$$

$$\tilde{\Delta} v' = \frac{\partial \omega_x'}{\partial z} - \frac{\partial \omega_z'}{\partial x} \tag{10e}$$

$$\frac{\partial^2 w'}{\partial x^2} + \frac{\partial^2 w'}{\partial z^2} = \frac{\partial \omega_y'}{\partial x} - \frac{\partial^2 v'}{\partial x \partial y} \tag{10f}$$

for the three velocity components. The Laplace operator is defined as

$$\tilde{\Delta} = \frac{1}{Re}\frac{\partial^2}{\partial x^2} + \frac{\partial^2}{\partial y^2} + \frac{1}{Re}\frac{\partial^2}{\partial z^2}$$

Equations (10a–10f) are solved with the following boundary conditions. At the upstream boundary ($x = x_0$), we assume that all disturbances are zero,

$$f'(x_0, y, z, t) = 0 \tag{11}$$

where f' denotes the variables u', v', w', ω_x', ω_y', and ω_z', respectively. At the wall, no-slip conditions are used, thus

$$u'(x, 0, z, t) = 0 \tag{12a}$$

$$w'(x, 0, z, t) = 0 \tag{12b}$$

The v'-velocity component is prescribed as a function of x, z, and t,

$$v'(x, 0, z, t) = f_v'(x, z, t) \tag{12c}$$

This allows the generation of disturbances in the integration domain by local time-dependent blowing and suction within a narrow strip at the wall as will be discussed later. The vorticity components are calculated from the following equations:

$$\frac{\partial^2 \omega_x'}{\partial x^2} + \frac{\partial^2 \omega_x'}{\partial z^2} = -\frac{\partial^2 \omega_y'}{\partial y \partial x} + \frac{\partial}{\partial z}\tilde{\Delta} v' \tag{12d}$$

$$\omega_y'(x, 0, z, t) = 0 \tag{12e}$$

$$\frac{\partial w_z'}{\partial x} = \frac{\partial \omega_x'}{\partial z} - \tilde{\Delta} v' \tag{12f}$$

At the outflow boundary, the disturbances are assumed to be spatially periodic with a wave number α (see Fasel et al.[5]), and hence Eqs. (10a–10f) are solved using

$$\left.\frac{\partial^2 f'}{\partial x^2}\right|_{x_N, y, z, t} = -\alpha^2 f'(x_N, y, z, t) \tag{13}$$

for each variable f'. The wave number α is an expected wave number for the disturbances (near the outflow boundary) resulting from the primary instability. The energetic scales resulting from the primary (and possible secondary) instability are considered the most difficult to pass through the outflow boundary without causing reflection. Our past experience with using α of the primary instability in Eq. (13) supports this expectation. Using this boundary condition, large-amplitude disturbances that are composed of nonlinearly generated disturbance components with different wave numbers cannot pass through the boundary without causing noticeable reflections. Therefore, as noted for previous calculations, the outflow boundary was moved ahead of the large amplified vortical entities propagating downstream after initiation. This is the region of dominant sources in Eq. (1). As discussed in Sec. I, their influence reaches all boundaries (after attenuation with distance), and all of the dipole reflections from the boundaries are unphysical. Therefore, to minimize reflections from the outflow condition, Eq. (13), or any equivalent one, the physical disturbances near the outflow boundary need to (and, as we shall see, can) be reduced to small levels. Such a reduction of these amplitudes can be achieved with measures described in the next section.

As for the base flow, we assume potential flow along the freestream boundary and thus

$$\omega_x'(x, y_M, z, t) = 0 \tag{14a}$$

$$\omega_y'(x, y_M, z, t) = 0 \tag{14b}$$

$$\omega_z'(x, y_M, z, t) = 0 \tag{14c}$$

For the v' component, exponential decay in the y direction is prescribed,

$$\left.\frac{\partial v'}{\partial y}\right|_{x, y_M, z, t} = -\frac{\alpha^*}{\sqrt{Re}} v'(x, y_M, z, t) \tag{14d}$$

where α^* is an expected wave number dependent on x.

For the spanwise boundaries at $z = 0$ and $z = \lambda_z$, periodicity conditions are employed. Thus, for all variables and their derivatives,

$$f'(x, y, 0, t) = f'(x, y, \lambda_z, t) \tag{15a}$$

$$\left.\frac{\partial^n f'}{\partial z^n}\right|_{x, y, 0, t} = \left.\frac{\partial^n f'}{\partial z^n}\right|_{x, y, \lambda_z, t}, \qquad n = 1, 2, \ldots \tag{15b}$$

are enforced.

Exploiting the periodic boundary condition, Eqs. (15a) and (15b), in the spanwise direction, a spectral ansatz can be introduced for all variables f':

$$f'(x, y, z, t) = \sum_{k=-K}^{K} F_k(x, y, t) e^{ik\gamma z} \tag{16}$$

The wave number γ is related to the spanwise wavelength by $\gamma = 2\pi/\lambda_z$. The F_k are the complex conjugates of the F_{-k}, and therefore Eqs. (10a–10f) can be transformed into $K + 1$ equations for a plane integration domain.

All derivatives with respect to x and y are discretized with fourth-order accurate finite difference approximations, and the integration in time is performed with a fourth-order accurate Runge-Kutta-Merson scheme. The nonlinear terms are computed using a pseudospectral method. For the solution of the v'-Poisson equation, a multigrid method is employed with a line-iteration technique for each grid that is similar to the one used for the base flow. The u'- and w'-Poisson equations are solved directly.

The disturbances are introduced through a narrow spanwise strip at the wall. Whereas in most experiments disturbances

are introduced by a vibrating ribbon, in our simulations the disturbances are introduced by time-periodic blowing and suction within the disturbance strip. This blowing and suction is also an effective method to produce Tollmien-Schlichting waves.[10] With a given frequency and spanwise wavelength, different kinds of two-dimensional and pairs of three-dimensional oblique Tollmien-Schlichting waves, as well as longitudinal vortices, can be generated. For the investigations in this paper we choose

$$f_v'(x, z, t) = [A_{2D} + A_{3D}\cos(\gamma z)]\sqrt{Re}\, f_x(x)\sin(\beta t) \quad (17)$$

where f_x is shown in Fig. 1 and A_{2D} and A_{3D} denote the two- and three-dimensional disturbance amplitudes, respectively. Flow visualizations of transition in adverse pressure gradient boundary layers without artificial forcing by Gad-el-Hak et al.[11] suggest that an assumption of the form of Eq. (17) is sufficient to initiate the key mechanisms.

III. Numerical Calculations

A. Test Case

As a test case for the various techniques of treating the region near the outflow boundary, the simulation of a fundamental resonance breakdown of a flat-plate boundary layer with a strong adverse pressure gradient (Hartree parameter $\beta_H = -0.18$) was chosen. In contrast to a zero pressure gradient flow, the amplification rates are very large. As mentioned, this leads to a short breakdown region, which saves computational costs. Furthermore, the spatial breakdown in boundary layers with large adverse pressure gradients has not been investigated numerically. The flow visualizations of Gad-el-Hak et al.[11] for the case of a temporally decelerating boundary layer provide us with an idea of what type of breakdown to expect.

To judge the effectiveness of the different methods to treat the outflow region, the calculations are compared with a reference case without any special treatment. For this reference case, the integration domain was extended in the downstream direction far enough to prevent the leading wave front from reaching the outflow boundary before a timewise periodic flow was established in the region of physical interest.

The flow parameters for the test case are shown in Table 1. Two disturbance modes were introduced downstream of the inflow boundary by time-periodic blowing and suction within the disturbance strip: a two-dimensional wave with the frequency parameter $F = 1.08$ and the amplitude $A_{2D} = 0.0001$ and a pair of oblique three-dimensional waves with identical frequency and amplitude $A_{3D} = A_{2D}$. The amplitude of the disturbance input is small enough to insure an initial linear disturbance development in the downstream direction. The physical aspects of the test case are summarized next for the reference calculation.

Table 1 Physical and numerical parameters for the simulations

Reference length	$L = 0.05$ m
Reference velocity	$U_\infty = 30$ m/s
Kinematic viscosity	$\nu = 1.5 \times 10^{-5}$ m^2/s
Global Reynolds number	$Re = 10^5$
Hartree parameter	$\beta_H = -0.18$
Position of inflow boundary	$x_0 = 1.5846$
Mesh size in streamwise direction	$\Delta x = 0.008434$
Height of the integration domain	$y_M = 34.79$
Mesh size in normal direction	$\Delta y = 0.36234$
Spanwise wave number	$\gamma = 30.62$
Number of modes [see ansatz, Eq. (16)]	$K = 2$
Disturbance region (see Fig. 1)	$x_1 = 2.082$, $x_2 = 2.285$
Disturbance frequency ($\beta = \bar{\beta}L/U_\infty$, $\bar{\beta}$-angular frequency)	$\beta = 10.8$
Frequency parameter ($F = \bar{\beta}L/U_\infty \times 10^4/Re$, $\bar{\beta}$-angular frequency)	$F = 1.08$
Disturbance amplitudes	$A_{2D} = 0.0001$, $A_{3D} = 0.0001$
Time step (largest, smallest)	$\Delta t = 0.01164$, 0.002909

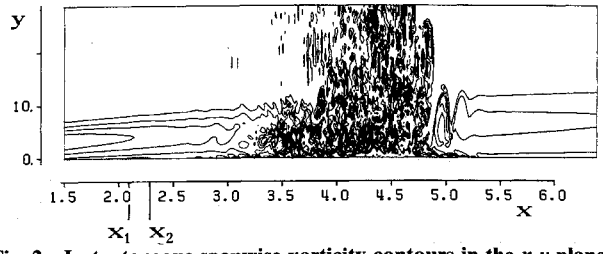

Fig. 2 Instantaneous spanwise vorticity contours in the x-y plane at $z = \lambda_z/2$ (case 1).

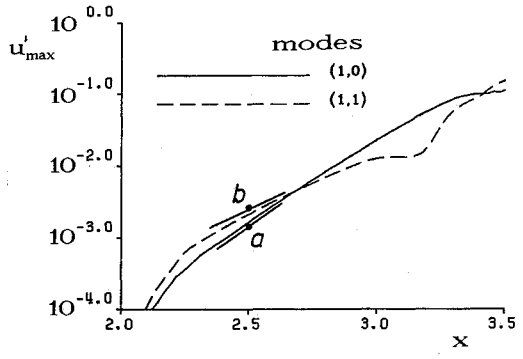

Fig. 3 Amplification curves of the maximum of the u' disturbances for the two-dimensional mode (1, 0) and for the three-dimensional mode (1, 1); a and b: growth rates of primary linear stability theory (parallel and spatial) at $x = 2.5$.

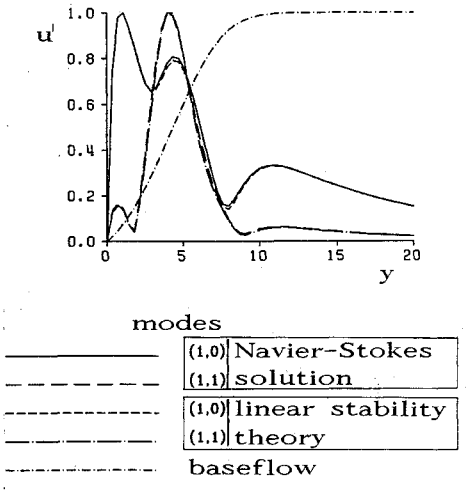

Fig. 4 Normalized amplitude distributions of the modes (1, 0) and (1, 1) and base flow profile at $x = 2.5$; comparison of Navier-Stokes solution (case 1) and linear stability theory.

B. Reference Case

Typical results of the reference calculation are presented in Figs. 2–7. An overall impression of the instantaneous flowfield can be obtained from Fig. 2, where lines of constant spanwise vorticity ω_z are shown. The flow attains a time-periodic state up to about $x = 4.0$, after seven disturbance periods, at the time when the simulation was stopped. Downstream of this region, the flow is nonperiodic and finally random in nature. Up to approximately $x = 3.0$, the generated Tollmien-Schlichting waves are monotonically amplified accordingly to the prediction of linear stability theory for the decelerated boundary layer (Fig. 3). The normalized ampli-

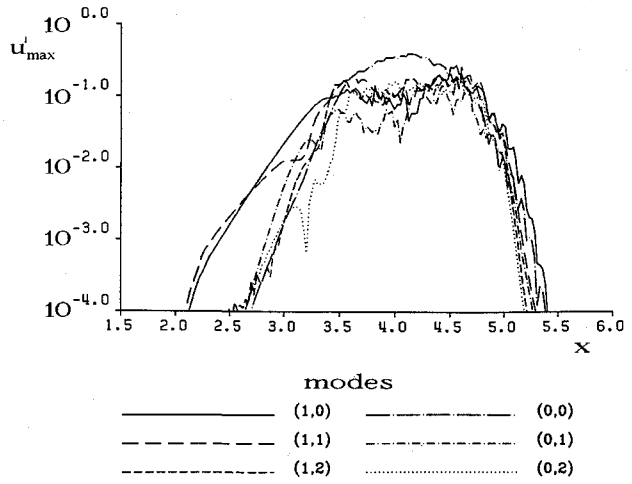

Fig. 5 Amplification curves of the maximum of the u' disturbances for different modes (case 1).

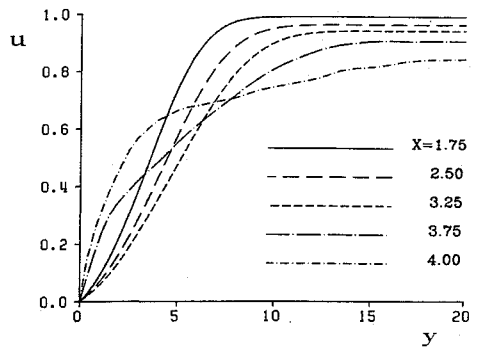

Fig. 6 Mean-flow u-velocity profiles at different x locations (case 1).

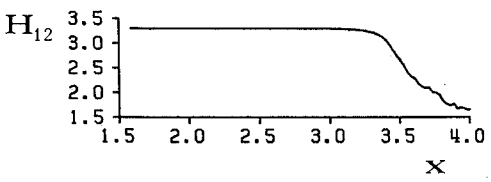

Fig. 7 Shape factor H_{12} vs x (case 1).

tude distributions for the u'-velocity component obtained from the Navier-Stokes calculation agree well with the results of a parallel linear stability analysis (Fig. 4). Downstream of $x = 3.0$, the fundamental three-dimensional mode (1, 1) undergoes enhanced amplification due to a resonant interaction with the two-dimensional mode (1, 0) (modes are labeled according to their position in the frequency-spanwise wave number spectrum relative to the corresponding disturbance values). The longitudinal vortex [mode (0, 1)], which is necessary for the nonlinear coupling mechanism, was nonlinearly generated by the modes (1, 0) and (1, 1). As can be seen in Fig. 5, at $x = 3.0$ the amplitude of this longitudinal vortex has grown to the level of the mode (1, 1), thus providing the conditions for the resonant interaction.

Also, at about $x = 3.5$, the disturbed and nonlinearly generated modes show saturation (Fig. 5) at an amplitude level of about 15% of the reference velocity U_∞, with a maximal change in the u_B base-flow profile (0, 0) of about 40%. Full breakdown to turbulence would probably occur here if the spatial resolution were fine enough. In this simulation, however, only three modes in the spanwise direction [$K = 2$ in Eq. (16)] were used. But, as can be observed in Fig. 6, downstream of $x = 3.75$ the mean-flow profile of the streamwise velocity component u exhibits a changeover to a shape typical of turbulent profiles. In addition, the shape factor H_{12} decreases for $H_{12} = 3.3$ for the laminar Falkner-Skan base flow to about $H_{12} = 1.6$ at $x = 4.0$ (Fig. 7). Of course, the disturbance behavior in the highly nonlinear regime (downstream of $x = 3.5$) has to be seen in a qualitative manner. Because of the coarse resolution, the simulation cannot reveal complete details of the breakdown to turbulence. More details and references for the case of a fundamental resonance breakdown of a strongly decelerated boundary layer are given by Kloker and Fasel.[12]

C. Treatment of Outflow Region

The numerical calculation described earlier was used as a reference case for other calculations, where different methods of treating the region near the outflow boundary were investigated. For these cases, an integration domain was used that was shorter than that of the reference case. Now, the disturbances *did* reach the outflow boundary where the amplitude level near the boundary depended on the measures applied. The various calculation cases, indicating the treatment of the outflow region, are listed next (more details are given in Table 2):

1) no treatment of outflow region; "long" integration domain (reference case)

2) no treatment of outflow region; "short" integration domain

3) acceleration of the base flow and local suction

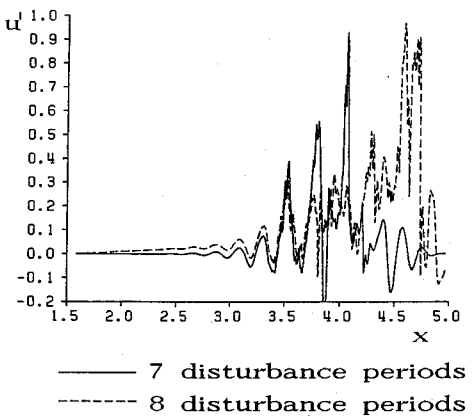

Fig. 8 Instantaneous signals of the u' disturbance at $y = 0.72$ and $z = 0$ for different time levels (case 2).

Table 2 Treatment of outflow region for the different simulation cases

Case	x_N[a]	x_i[b]	Measures taken in outflow region[c]
1	6.316	—	—
2	4.967	—	—
3	4.967	4.106	u_B velocity at the upper boundary, Eq. (9b) is continuously increased from $u_B(x_i) = 0.926$ to $u_B(x_N) = 1.067$ according to a Hartree parameter $\beta_H = 1.0$ downstream of x_i, suction is applied from x_i to $x = 4.314$ with a volume flow of $\dot{m} = -0.000791$
4	4.967	4.106	Same as for case 3 plus linearized equations starting from x_i
5a	4.967	3.600	Viscosity is increased by a factor of 100 from x_i to $x = 3.811$
5b	4.967	3.600	Viscosity is increased by a factor of 1000 as for case 5a
6	4.967	4.494	Disturbance vorticity is weighted with the function F_D shown in the lower part of Fig. 10b

[a] x_N—position of outflow boundary.
[b] x_i—start of outflow region.
[c] All changes in the flow imposed in x direction at the beginning of the influence zone are smooth up to the second derivative. This is achieved by connecting different functions with a parabola of 5th order.

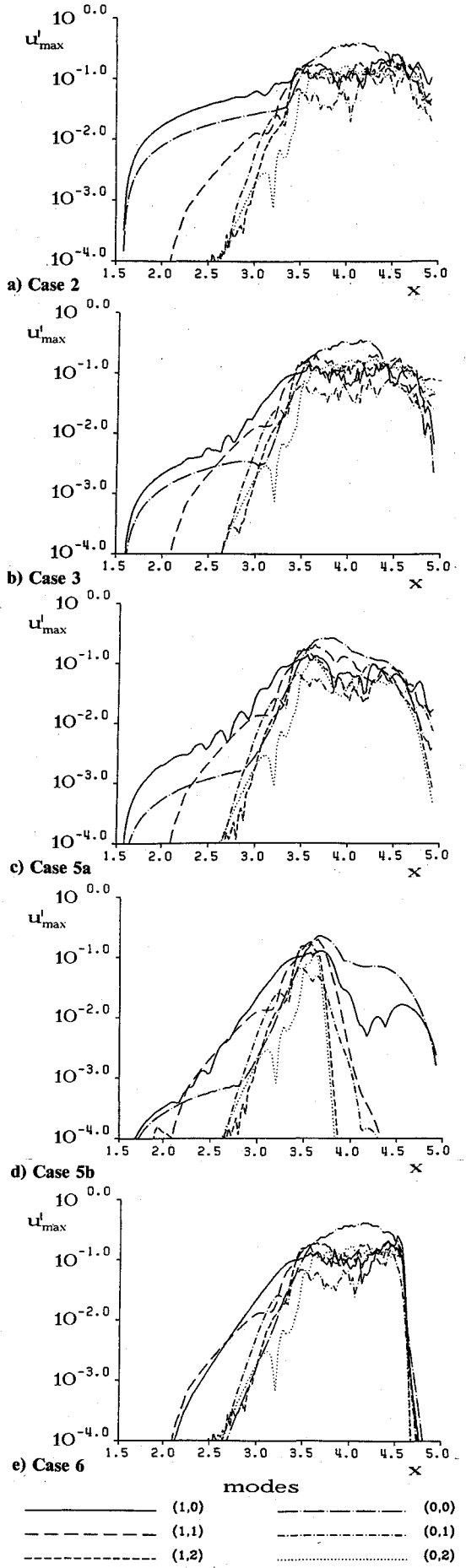

Fig. 9 Amplification curves of the maximum of the u' disturbances for different modes.

4) acceleration of the base flow, local suction, and linearized equations
5) increased viscosity
6) gradually suppressed disturbance vorticity

The effects of the various measures are discussed subsequently.

D. Numerical Results and Comparison

The instantaneous u'-velocity signal over x (at a fixed y and z position) of calculation case 2 is shown in Fig. 8 after a calculation time of seven and eight disturbance periods. After the seventh period, the disturbances have not yet reached the outflow boundary ($x_N = 4.967$), whereas one period later the leading wave front has already started to pass through the boundary. Physically, the two signals should coincide up to $x = 3.5$ due to the time-periodic behavior in this early transition stage. Obviously, at the later time level, there is an extra-strong upstream effect induced by the leading vorticity wave front passing through the outflow boundary. A comparison of the downstream development of the maximal u' amplitudes for the different modes (Fig. 9a) with that of the reference case (Fig. 5) reveals the drastic upstream contamination, in particular on the two-dimensional modes (1, 0) and (0, 0) between $x = 1.58$ and 3.5. Therefore, in the following, the behavior of the mode (1, 0) upstream of $x = 3.5$ is used to validate the efficiency of the various methods of treating the outflow region. The only explanation for the growth of this mode and for the mean-flow change *upstream* of the wall excitation slot

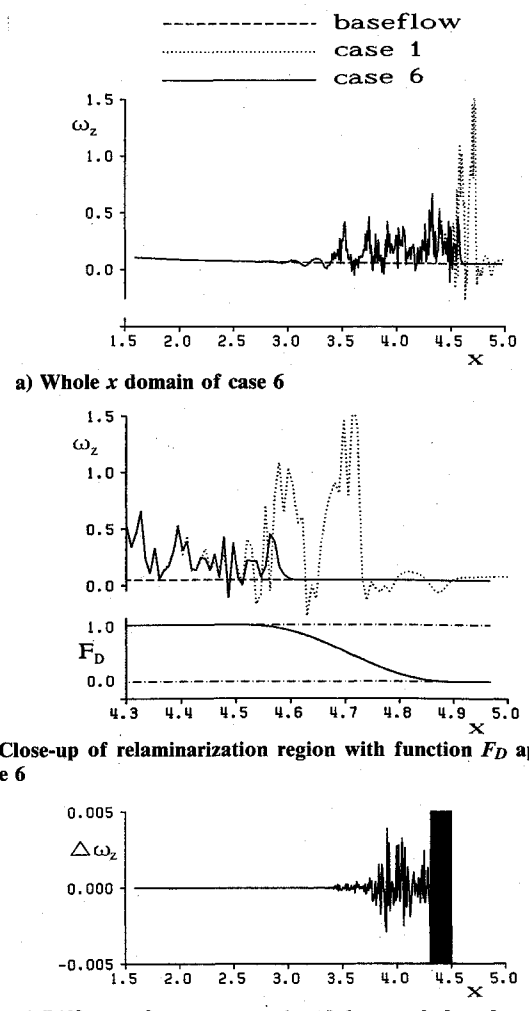

Fig. 10 Comparison of the instantaneous total spanwise vorticity ω_z signals of cases 1 and 6 after eight disturbance cycles at $y = 0.72$ and $z = 0$.

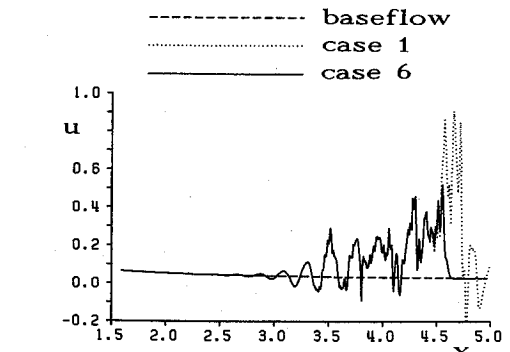

a) Whole x domain of case 6

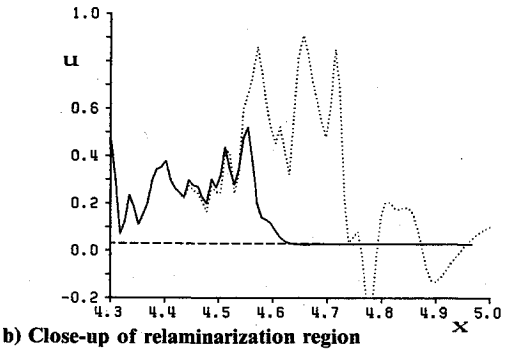

b) Close-up of relaminarization region

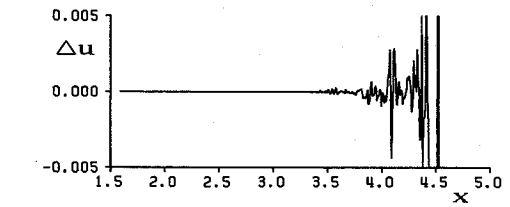

c) Difference between cases 1 and 6 over whole x domain

Fig. 11 Comparison of the instantaneous total streamwise velocity u signals of cases 1 and 6 after eight disturbance cycles at $y = 0.72$ and $z = 0$.

appears to be the buildup of a global instability by continued reflection and re-reflections of pressure fields between the inflow and outflow boundaries, alluded to in Sec. I. The seemingly disorganized vorticity field of Fig. 2 contains large-scale, nearly regular, oscillatory and mean-flow structures. Of these, the two-dimensional modes reflect most efficiently and should become dominant in global instabilities (if any develop).

In case 3, acceleration of the boundary layer (corresponding to a Hartree parameter $\beta_H = 1.0$) and additional suction at the wall were applied in the outflow region. This resulted in a reduction of the disturbance level at the outflow boundary by a factor of about 10 (Fig. 9b). Evidently the reduction of the disturbances arriving at the outflow does not prevent the global instability buildup upstream of the excitation slot. The global instability merely saturates at lower amplitudes. An additional linearization of the vorticity transport equations within the outflow region (case 4), to fully exploit the stabilizing effects of acceleration and suction as predicted by linear theory, leads only to minor improvements.

Imposing an artificial increase of the viscosity downstream of $x = 3.6$ by a factor of 100 (case 5a, Fig. 9c) or 1000 (case 5b, Fig. 9d) is more effective. The high viscosity strongly damps the three-dimensional fluctuations (1, 1) and (1, 2), as well as the longitudinal vortices (0, 1) and (0, 2) in Fig. 9d. However, pressure feedback upstream of the slot persists, though palpably diminished. A further increase of viscosity may suppress the levels further. However, in our explicit numerical method, the viscous time step restriction enforces a reduction of the time step proportional to the viscosity increase. If this restriction falls below the convective limit, which sets the bound for the time step in our numerical scheme without additional viscosity, the overall efficiency of the method is compromised.

Detailed analysis of the results of cases 2–5 reveals that the upstream effect of any disturbances passing the outflow boundary is directly dependent on their amplitudes at the outflow boundary. The physical means of stabilization discussed earlier were not efficient enough to reduce these disturbance levels to values low enough for the upstream reflections and re-reflections to become negligible, at least not without an increase in computing cost (either by requiring smaller time steps or using an extended outflow region).

The results obtained from case 5, where the viscosity was increased, led to the idea of influencing the disturbances *directly* to suppress the fluctuations. Thus the time step restriction mentioned earlier would be avoided. Furthermore, various numerical tests have shown that the disturbance flow in the outflow region should be treated such that the continuity condition is always preserved. Otherwise, infinitely fast propagating, sound-like disturbances may contaminate the flow-

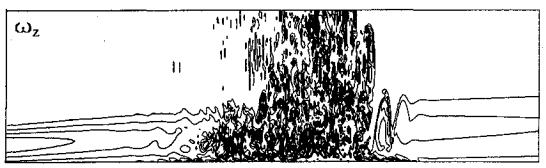

a) Case 1 (reference case, long integration domain)

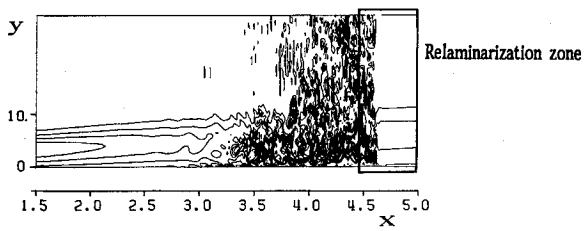

b) Case 6 (short integration domain with relaminarization zone)

Fig. 12 Instantaneous spanwise vorticity ω_z contours in the x-y plane at $z = \lambda_z/2$ after eight disturbance cycles.

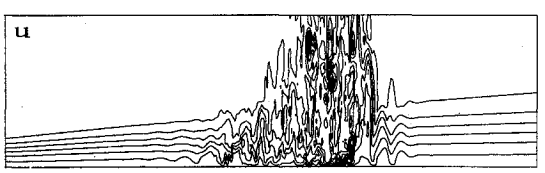

a) Case 1 (reference case, long integration domain)

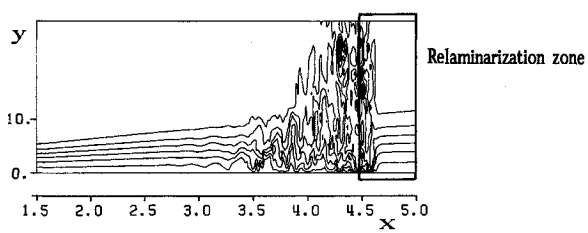

b) Case 2 (short integration domain with relaminarization zone)

Fig. 13 Instantaneous streamwise velocity u contours in the x-y plane at $z = \lambda_z/2$ after eight disturbance cycles.

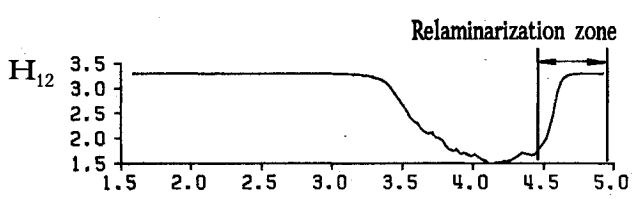

Fig. 14 Shape factor H_{12} vs x for simulation case 6.

field. In our formulation of the Navier-Stokes equations, we can directly influence the disturbance *vorticity* alone while preserving continuity and minimizing pressure disturbances. In the calculation of case 6, the vorticity components are spatially suppressed in the outflow region by multiplying them with a weighting function $F_W(x, y, z) = F_D(x)$ after each (intermediate) time step. The function $F_D(x)$ is 1 at the beginning of the relaminarization zone and decreases gradually to 0 at a few grid points upstream of the actual outflow boundary x_N. The velocity components are calculated in the same way as in the remainder of the integration domain, namely using the Poisson-type equations, Eqs. (10d–10f), which satisfy implicitly the continuity condition. The gradual decay of the right-hand sides of Eqs. (10d–10f) in the relaminarization zone then enforces the decay of the velocity components. Results for case 6 are shown in Figs. 9e–12.

The weighting function for reducing the disturbance vorticity in the outflow region is shown in the lower part of Fig. 10b. As can be seen in Fig. 9e, all u'-fluctuation amplitudes decay rapidly to very low values. The comparison of the results with case 1 (Fig. 5) does not exhibit any significant difference in the u' amplitudes upstream of about $x = 4.5$. In Figs. 10a and 10b, the instantaneous total vorticity component ω_z close to the wall ($y = 0.72$) at $z = 0$ is plotted after the eighth period for both case 6 and reference case 1. Corresponding plots for the total streamwise velocity component are given in Figs. 11a and 11b. Comparison of the curves for calculation cases 1 and 6 demonstrates the drastic decay of the vorticity and velocity disturbances and shows that the signals are practically identical upstream of about half a wavelength from the beginning of the relaminarization zone. Even when taking extremely small differences into consideration, as shown in Fig. 10c, differences are discernible only up to $x = 3.5$. Obviously, these extremely small differences are hardly relevant to the main mechanisms. The upstream effect may be even smaller in a flow with a zero or negative streamwise pressure gradient because of the smaller effect of the pressure feedback mechanism. An enhanced impression of the efficiency of the artificially forced relaminarization process is obtained from Figs. 12 and 13, where contour plots of the instantaneous vorticity ω_z and velocity u in the x-y plane at $z = \lambda_z/2$ are shown for cases 1 and 6. Finally, Fig. 14 further documents the relaminarization process by the rapid increase of the integral boundary-layer parameter H_{12} from about 1.6 back to the laminar value of 3.3.

The contrast in the efficiency of the vorticity suppression zone and the other strategies is striking (compare Figs. 9a–9e). The comparison of the reference flowfields with those using the vorticity suppression zone in Figs. 10–13 suggests that, although none of the flowfields is truly physical, both calculations, cases 1 and 6, capture correctly the dominant mechanisms of early transition.

IV. Conclusions

In this paper, we presented various measures to treat the outflow region for direct numerical simulations of laminar-turbulent transition in spatially evolving boundary layers based on the Navier-Stokes equations. These measures are aimed at relaxing the highly fluctuating flow in the region near the outflow boundary of the integration domain to a practically steady laminar state. Then the calmed flow should pass through the outflow boundary region without causing significant upstream reflections. Our numerical experiments were consistent with the theoretical framework for simple and zone boundaries outlined in Sec. I. Both types of boundaries can contribute to the generation of unphysical pressure fields that propagate to the inflow boundary and reflect back and forth. In our case of an adverse pressure gradient, which is a severe test of the procedure, substantial coherent vortical structures are present even when the computed flowfields appear disorganized. Of these structures, two-dimensional modes are reflected most efficiently and apparently build globally unstable fields with different saturation levels of disturbance. Among the techniques tried, that of the vorticity-suppression zone evidently succeeded in keeping the disturbances below the nonlinear threshold level necessary for global instability. Analytical proofs of such behavior are unlikely to be forthcoming in the near future. Thus we must rely on numerical evidence, such as provided in Figs. 10 and 11. In our formulation of the governing equations in terms of vorticity, supression of all components of fluctuating vorticity can be achieved easily at successive grid points within a "relaminarization zone" near the outflow boundary. With this procedure, practically total dissipation of all disturbances can be accomplished without violating the continuity condition and without imposing any additional restrictions on the usable step size for the time integration. The procedure should be even more effective in more stable wall layers. It also holds promise for applications to the more unstable free shear layers, wakes, and jets.

Acknowledgments

This paper benefited from the combined experience of many years of research sponsored by different agencies, mainly by the Deutsche Forschungsgemeinschaft and the Stiftung Volkswagenwerk in Germany and the Office of Naval Research in the United States (Contracts N00014-K-0515 and N00014-T-1274). The third author would like to express special thanks to a very special friend, M. V. Morkovin, who has contributed immensely to this paper through stimulating discussions of this topic over a span of many years, starting in 1978 and up to the actual preparation of this paper.

References

[1]Kleiser, L., and Zang, T. A., "Numerical Simulation of Transition in Wall-Bounded Shear Flows," *Annual Review of Fluid Mechanics*, Vol. 23, 1991, pp. 495–538.

[2]Buell, J. C., and Huerre, P., "Inflow/Outflow Boundary Conditions and Global Dynamics of Spatial Mixing Layers," *Proceedings of Summer Program 1988*, Center for Turbulent Research, NASA Ames Research Center, 1988, pp. 19–26.

[3]Huerre, P., and Monkewitz, P. A., "Local and Global Instabilities in Spatially Developing Flows," *Annual Review of Fluid Mechanics*, Vol. 22, 1990, pp. 473–538.

[4]Grinstein, F. F., Orom, E. S., and Boris, J. P., "Pressure Field, Feedback, and Global Instabilities of Subsonic Spatially Developing Mixing Layers," *Physics of Fluids A*, Vol. 3, 1991, pp. 2401–2409.

[5]Fasel, H., Rist, U., and Konzelmann, U., "Numerical Investigation of the Three-Dimensional Development in Boundary-Layer Transition," *AIAA Journal*, Vol. 28, No. 1, 1990, pp. 29–37.

[6]Konzelmann, U., Rist, U., and Fasel, H., "Numerical Investigation of the Effects of Longitudinal Vortices on the Onset of Transition in a Flat Plate Boundary Layer," *Proceedings of the AGARD Conference on Fluid Dynamics of Three-Dimensional Turbulent Shear Flows and Transition* (Cesme, Turkey), AGARD-CP-438, 1989, pp. 7/1–13.

[7]Spalart, P. R., "Direct Numerical Study of Leading Edge Contamination," *Proceedings of the AGARD Conference on Fluid Dynamics of Three-Dimensional Turbulent Shear Flows and Transition*, (Cesme, Turkey), AGARD CP-438, 1989, pp. 5/1–13.

[8]Spalart, P. R., "Direct Numerical Study of Crossflow Instability," *Proceedings of the 3rd IUTAM Symposium on Laminar-Turbulent Transition* (Toulouse, France), edited by R. Michel and D. Arnal, Springer-Verlag, 1990.

[9]Fasel, H., "Investigation of the Stability of Boundary Layers by a Finite-Difference Model of the Navier-Stokes Equations," *Journal of Fluid Mechanics*, Vol. 78, 1976, pp. 355–383.

[10]Kozlov, V. V., and Levchenko, V. Y., "Laminar-Turbulent Transition Control by Localized Disturbances," *Proceedings of the IUTAM Symposium on Turbulence Management and Relaminarisation* (Bangalore, India), edited by H. W. Liepmann and R. Narasimha, Springer-Verlag, 1988.

[11]Gad-el-Hak, M., Davis, S. H., McMurray, J. T., and Orszag, S. A., "On the Stability of the Decelerating Laminar Boundary Layer," *Journal of Fluid Mechanics*, Vol. 138, 1984, pp. 297–323.

[12]Kloker, M., and Fasel, H., "Numerical Simulation of Two- and Three-Dimensional Instability Waves in Two-Dimensional Boundary Layers with Streamwise Pressure Gradient," *Proceedings of the 3rd IUTAM Symposium on Laminar-Turbulent Transition* (Toulouse, France), edited by R. Michel and D. Arnal, Springer-Verlag, 1990.